

GALAXYDiT: Efficient Video Generation with Guidance Alignment and Adaptive Proxy in Diffusion Transformers

Zhiye Song¹, Steve Dai², Ben Keller², Bruce Khailany²

¹Massachusetts Institute of Technology, ²NVIDIA

¹zhiye@mit.edu, ²{sdai, benk, bkhalany}@nvidia.com

Abstract

Diffusion models have revolutionized video generation, becoming essential tools in creative content generation and physical simulation. Transformer-based architectures (DiTs) and classifier-free guidance (CFG) are two cornerstones of this success, enabling strong prompt adherence and realistic video quality. Despite their versatility and superior performance, these models require intensive computation. Each video generation requires dozens of iterative steps, and CFG doubles the required compute. This inefficiency hinders broader adoption in downstream applications.

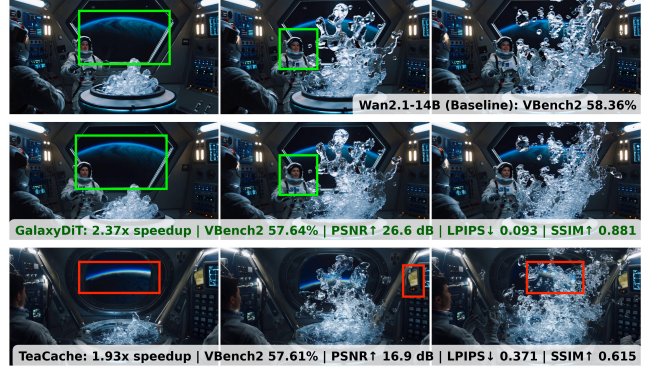
We introduce GALAXYDiT, a training-free method to accelerate video generation with guidance alignment and systematic proxy selection for reuse metrics. Through rank-order correlation analysis, our technique identifies the optimal proxy for each video model, across model families and parameter scales, thereby ensuring optimal computational reuse. We achieve 1.87× and 2.37× speedup on Wan2.1-1.3B and Wan2.1-14B with only 0.97% and 0.72% drops on the VBench-2.0 benchmark. At high speedup rates, our approach maintains superior fidelity to the base model, exceeding prior state-of-the-art approaches by 5 to 10 dB in peak signal-to-noise ratio (PSNR).

1 Introduction

Diffusion models have revolutionized image and video generation, with unprecedented capabilities in creative content production and physical world simulation [11, 15, 16]. Applications of video diffusion models range from entertainment and advertising to synthetic data generation for autonomous driving and robotics. Diffusion models work by learning to predict the noise that has been gradually added to videos; during inference, they progressively remove noise to generate coherent video content during iterative steps.

Diffusion transformers (DiTs), initially proposed for image generation [13], have become the foundation of modern video generation models [5, 11, 14, 16, 18]. Recent state-of-the-art models, such as Wan2.1 [16] and COSMOS [11], have demonstrated the superior performance of the DiT architecture. Classifier-free guidance (CFG) [1] has become essential for these models [5, 11, 16], achieving superior prompt adherence and video quality. These models can capture complex attributes including physical laws, commonsense reasoning, and compositional integrity, as evidenced by the VBench-2.0 benchmark [23]. This progression from superficial properties to modeling complex real-world phenomena makes video diffusion increasingly valuable for downstream applications.

However, the compute cost of DiT-based video generation hinders broader adoption. Each denoising step, or sampling step, requires dozens of Tera-FLOPs, and dozens of steps are required to produce a single video. This cost is further amplified by CFG, which



Prompt: A space station interior with microgravity conditions, where a bottle of water is opened... Astronauts in space suits observe the phenomenon, **their faces reflecting curiosity and amazement**. The background shows the station's control panels and windows revealing a distant planet or galaxy...

Figure 1: Visual comparison of the Wan2.1-14B model, GALAXYDiT-fast, and prior work [7]. Metrics shown are for the full benchmark evaluation. Best viewed zoomed in.

runs two parallel diffusion passes at each denoising step. With these computational needs, Wan2.1-14B takes 7 minutes to generate a 5-second video clip on 8 A100 GPUs.

One promising approach to reduce computation without additional training is reuse, taking advantage of the similarities between adjacent denoising steps by saving intermediate data for later reuse. Despite feature similarities, deciding when to reuse is critical to maintain output quality. The optimal reuse opportunity differs widely across models and across prompts due to different noise schedulers, video encoders, model architectures, and parameters. Prior works have proposed a one-size-fits-all approach, using the same reuse metric for different models [7]. However, we observe that the statistics used to calculate the reuse metric, i.e. proxies, vary across model families and scales, suggesting that a systematic approach to select the model-specific optimal reuse metric is essential.

Moreover, existing techniques treat the conditional and unconditional passes of CFG independently during reuse decisions. This misaligns the noise predictions and produces visual artifacts. Since CFG is essential for high-quality generation, developing a CFG-aware reuse strategy presents a critical opportunity for efficient video generation.

To address these challenges, we propose GALAXYDiT, a training-free reuse method to accelerate video generation. Our contributions are:

- We demonstrate that different models have different proxies that correlate best with the ideal reuse metric (i.e., the oracle).

- We design a proxy selection method using Spearman’s rank correlation coefficient to identify the best proxy for each model.
- We propose CFG-aligned reuse to eliminate visual artifacts caused by CFG-agnostic reuse methods.
- We present extensive evaluations across model architectures and parameter scales. GALAXYDiT-fast achieves 2.57×, 2.37×, 2.13× speedups on Wan2.1-1.3B, Wan2.1-14B, and Cosmos-Predict2-2B, respectively, with high fidelity to the base model, as measured by multiple full-reference metrics.

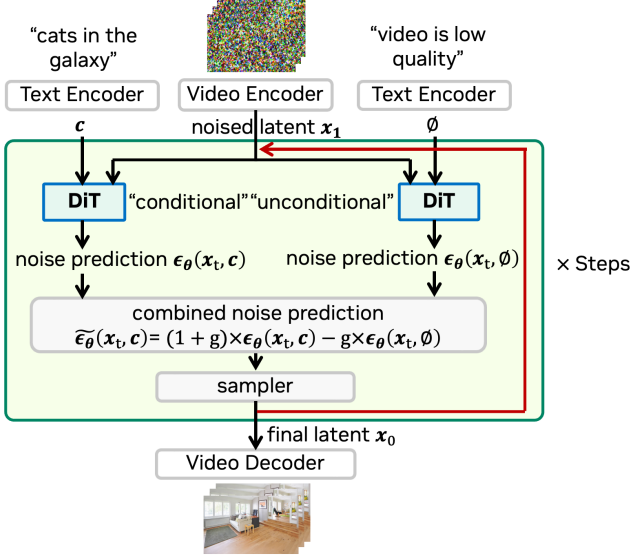


Figure 2: Video generation relies on diffusion transformers (DiTs) and classifier-free guidance (CFG).

2 Background

2.1 Video Generation with DiT and CFG

Transformer-based architecture (DiTs) and classifier-free guidance (CFG) have enabled the vast improvement in video generation [1, 2]. As shown in Figure 2, video generation is controlled through a condition vector c , typically text embeddings. Each DiT block processes the entire token sequence, through attention, cross-attention, and MLP layers. CFG [1] runs two parallel passes, conditional (with c) and unconditional (with \emptyset), then combines their noise predictions to achieve superior prompt adherence and video quality. The combined prediction is then fed to the sampler, which generates the next iteration’s input. Various noise schedulers [6, 8, 15] can be used to control the noise level at each denoising step.

2.2 Related Work

Several techniques have been proposed to reduce computation in DiT-based video generation. Model distillation approaches train student models that require fewer denoising steps. For example, AccVideo [21] trains the student model with a synthetic dataset generated by the teacher model. MCM [20] incorporates an additional high-quality image dataset to compensate the visual quality loss of

the individual frames. However, distillation is compute-intensive, requiring dozens of days on 8 A100 GPUs [21].

Training-free approaches avoid this cost. RADiT [12] skips layers when input features resemble the previous denoising step. However, it incurs significant memory cost when extended to larger models. For Wan2.1-14B, the 173 GB memory overhead makes it impossible to fit on a single A100 GPU. Similarly, the residual caching technique of DiTFastAttn [19] saves the attention layer output, translating to 58 GB memory overhead. FasterCache [9] exploits feature similarity between CFG’s conditional and unconditional passes, proposing frequency-based reuse for unconditional features, though this by design limits speedup to 2×. TeaCache [7] skips steps if the polynomial fit of the embedded input is greater than a threshold. Its extension to CFG-based models introduces visual artifacts, as will be discussed in Section 3.3. Sparsity-based approaches, such as Sparse VideoGen [17] that uses temporal and spatial sparsity patterns, are orthogonal and can be used together with reuse-based methods.

2.3 Full-Reference Video Quality Metrics

We compare latency-optimized models against base models using standard full-reference metrics: peak signal-to-noise ratio (PSNR) for absolute reconstruction error, structural similarity index measure (SSIM) for perceived structural changes, and learned perceptual image patch similarity (LPIPS) [22] for perceptual loss.

3 GALAXYDiT

3.1 Algorithm Overview

GALAXYDiT accelerates video generation through two key innovations: adaptive proxy selection and guidance-aligned reuse. The core insight is that not all denoising steps contribute equally to the final video quality, enabling video-dependent selective computation reuse between adjacent steps.

Our method operates in two phases: an offline proxy selection process and runtime inference acceleration. First, the proxy selection method (Section 3.2) identifies the optimal reuse metric for each model by analyzing rank-order correlations between candidate proxies and the oracle, which is an ideal metric of how important the current step is to the denoising process. This model-specific selection is crucial because different architectures and scales exhibit varying correlation patterns across their internal representations.

During inference, we use the selected proxy to determine when to skip computation at each denoising step. At the beginning of each step, we compute only a portion of the first DiT block of the conditional pass and extract the chosen proxy (Algorithm 1, line 3). We calculate the reuse metric by comparing the current proxy to the previous step’s proxy, normalized by the current proxy’s magnitude (line 4). This metric accumulates across steps to track the cumulative change since the last full computation. If this accumulated metric exceeds a threshold and we are past the initial 20% of denoising steps, we reuse cached residuals from the previous step for both conditional and unconditional passes (lines 6-8). Otherwise, we perform full computation for both passes and store the residuals for potential future reuse (lines 11-14).

A critical aspect of our approach is guidance alignment (Section 3.3). Unlike prior work that makes independent reuse decisions

for conditional and unconditional passes, we synchronize these decisions based on the conditional pass’s proxy. This ensures that the conditional and unconditional noise predictions, $\epsilon_\theta(\mathbf{x}_t, \mathbf{c})$ and $\epsilon_\theta(\mathbf{x}_t, \emptyset)$, used in CFG calculation (line 16), remain aligned at each denoising step, eliminating visual artifacts caused by misaligned guidance.

Algorithm 1 Video Generation Accelerated by GALAXYDiT

```

1: for denoising step  $S = 1$  to  $N_{\text{steps}}$  do
2:    $\triangleright$  Run the first DiT block of the conditional generation
3:    $\text{proxy}_S \leftarrow \text{DiTBlock0}(\mathbf{x}_t, \mathbf{c})$ 
4:    $\text{reuse\_metric} \leftarrow \text{reuse\_metric} + \frac{\|\text{proxy}_{S-1} - \text{proxy}_S\|_1}{\|\text{proxy}_S\|_1}$ 
5:    $\text{use\_cache} \leftarrow S > N_{\text{steps}} \times 0.2$  and  $\text{reuse\_metric} < \text{threshold}$ 
6:   if  $\text{use\_cache}$  then
7:      $\epsilon_\theta(\mathbf{x}_t, \mathbf{c}) \leftarrow \text{unpatchify}(\mathbf{y}_{\text{in}, S, \text{cond}} + \text{res}_{\text{cond}, S-1})$ 
8:      $\epsilon_\theta(\mathbf{x}_t, \emptyset) \leftarrow \text{unpatchify}(\mathbf{y}_{\text{in}, S, \text{uncond}} + \text{res}_{\text{uncond}, S-1})$ 
9:   else
10:     $\text{reuse\_metric} \leftarrow 0$ 
11:     $\epsilon_\theta(\mathbf{x}_t, \mathbf{c}) \leftarrow \text{DiT}(\mathbf{x}_t, \mathbf{c})$   $\triangleright$  Run full conditional pass
12:     $\text{res}_{\text{cond}, S-1} \leftarrow \mathbf{y}_{\text{out}, S} - \mathbf{y}_{\text{in}, S}$   $\triangleright$  occurs in the DiT
13:     $\epsilon_\theta(\mathbf{x}_t, \emptyset) \leftarrow \text{DiT}(\mathbf{x}_t, \emptyset)$   $\triangleright$  Run full unconditional pass
14:     $\text{res}_{\text{uncond}, S-1} \leftarrow \mathbf{y}_{\text{out}, S} - \mathbf{y}_{\text{in}, S}$   $\triangleright$  occurs in the DiT
15:   end if
16:    $\hat{\epsilon}_\theta(\mathbf{x}_t, \mathbf{c}) = (1 + g) \times \epsilon_\theta(\mathbf{x}_t, \mathbf{c}) - g \times \epsilon_\theta(\mathbf{x}_t, \emptyset)$ 
17:    $\mathbf{x}'_t \leftarrow \text{sampler}(\hat{\epsilon}_\theta(\mathbf{x}_t, \mathbf{c}), t)$ 
18: end for

```

3.2 Adaptive Reuse Metric

3.2.1 The Oracle. In an ideal scenario, we would have access to an "oracle", a metric quantifying the importance of each denoising step. We define this oracle as the relative change in residuals between consecutive steps, where the residual is the difference between the output and input of the DiT blocks, $\mathbf{y}_{\text{out}} - \mathbf{y}_{\text{in}}$ (Figure 3). This residual quantifies the transformation applied by the DiT at each step. A larger change indicates that it is more critical for final video quality.

By comparing the oracle to a threshold, we can partition denoising steps into two sets: steps with insignificant changes that can be safely reused, and important steps requiring full computation. Quantitatively, at sampling step S , the oracle is:

$$\text{Oracle}_S = \frac{\|(\mathbf{y}_{\text{out}, S} - \mathbf{y}_{\text{in}, S}) - (\mathbf{y}_{\text{out}, S-1} - \mathbf{y}_{\text{in}, S-1})\|_1}{\|(\mathbf{y}_{\text{out}, S} - \mathbf{y}_{\text{in}, S})\|_1} \quad (1)$$

where \mathbf{y}_{out} and \mathbf{y}_{in} are the output and input of the DiT blocks.

3.2.2 Proxy Candidates. In practice, computing the oracle requires a full forward pass through the DiT to obtain \mathbf{y}_{out} , defeating the purpose of reuse. We therefore introduce lightweight proxies that approximate the oracle by computing only the first DiT block and collecting intermediate statistics, requiring less than 1% of the full step computation.

Different models exhibit distinct internal dynamics during denoising. The self-attention, cross-attention, and MLP layers evolve differently across architectures and scales. Noise schedulers, which decides the amount of noise at each step, and adaptive layer norm

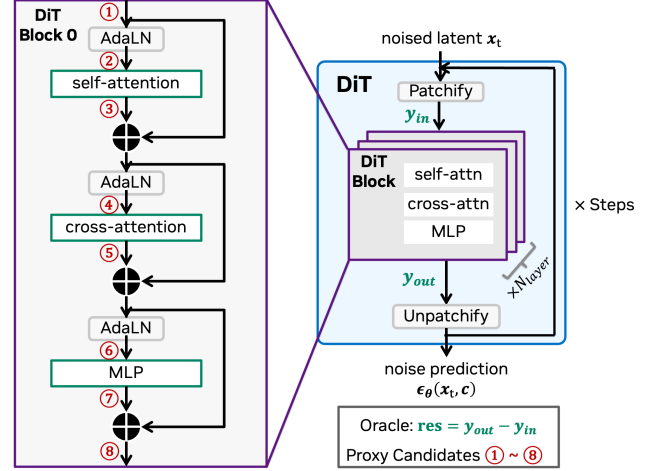


Figure 3: The oracle requires full DiT pass; various proxy candidates (names are labeled in Table 1) are intermediate tensors extracted from the first DiT block to approximate the oracle.

(AdaLN) further complicate these interactions. These architectural variations mean that different intermediate tensors correlate best with step importance across models. Thus, a proxy that effectively predicts importance in one model may fail in another.

We propose eight proxy candidates extracted from various points in the first DiT block, as labeled in Figure 3. Each proxy defines a corresponding reuse metric:

$$\text{Reuse metric}_S = \frac{\|\text{proxy}_{S-1} - \text{proxy}_S\|_1}{\|\text{proxy}_S\|_1}. \quad (2)$$

3.2.3 Proxy Selection. The key challenge is selecting the proxy that best approximates the oracle. In an ideal scenario, we would decide whether to reuse a denoising step by comparing the oracle against a threshold. In practice, we instead compare the reuse metric against another threshold.

The reuse metric’s threshold does not need to numerically match the oracle’s threshold. What matters is rank-order preservation: if the oracle indicates step A is less important than step B, the reuse metric should also rank step A lower than step B. This consistent ordering ensures we skip the same set of steps regardless of the absolute metric values, as long as both the oracle and the proxy partition the steps at similar positions in their respective rankings.

To quantify order preservation, we use Spearman’s rank correlation coefficient ρ , which evaluates the order-preserving nature of two data sets. Spearman’s ρ is equivalent to the Pearson correlation of the rank values of two variables:

$$\rho = 1 - \frac{6 \sum_{i=1}^n d_i^2}{n(n^2 - 1)}, \quad (3)$$

where $d_i = \text{rank}(x_i) - \text{rank}(y_i)$ represents the rank disagreement between corresponding elements of the two datasets.

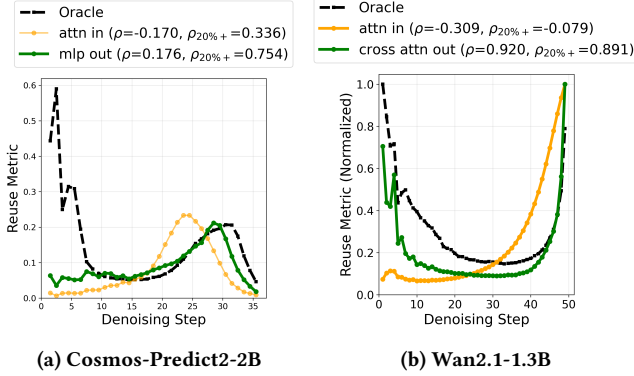


Figure 4: The comparison of two proxy candidates against the oracle for an example prompt. The optimal proxy candidate for each model is shown in green. A suboptimal proxy candidate is shown in orange.

In our context, we compute ranks across the denoising steps of a single video generation. Specifically, for each step $i \in \{1, \dots, N_{\text{steps}}\}$:

$$d_i = \text{rank}(\text{oracle}_i) - \text{rank}(\text{reuse metric}_i). \quad (4)$$

A high Spearman’s ρ (close to 1) indicates that the proxy candidate preserves the oracle’s ordering, making it suitable for our method. We compute ρ for each proxy candidate across a small number of prompts and select the proxy with the highest average correlation as the optimal choice for that model.

3.2.4 Proxy Selection Results. Figure 4 visualizes how different proxy candidates compare to the oracle in two model families. For Cosmos-Predict2 (Figure 4a), `mlp out` coincides closely with the oracle, while `attn in` peaks earlier, failing to capture the oracle’s behavior. Due to the lack of proxies reflecting the oracle at early steps, we exclude the first 20% of steps from reuse consideration, improving Spearman’s ρ from 0.176 to 0.754. This exclusion strategy is adopted across all models. For Wan2.1-1.3B (Figure 4b), `cross attn out` serves as the best oracle indicator.

Our analysis reveals two critical findings. First, the optimal proxy exhibits consistency across prompts within the same model. For Wan2.1-1.3B, $\rho_{\text{cross attn out}}$ achieves a mean of 0.89 with a standard deviation of only 0.11, demonstrating strong prompt-independent correlation. Second, as shown in Table 1, the three models have three different optimal proxies. These results underscore the necessity of model-specific proxy selection. Using a suboptimal proxy can severely degrade performance. For instance, applying the `mlp out` (optimal for Predict2) to Wan2.1-14B yields a weak correlation of only $\rho = 0.21$, making it unsuitable for reliable reuse decisions.

3.3 Guidance-Aligned Reuse

Prior work typically determines step skipping independently for the conditional and unconditional passes [7]. However, this independence causes visual artifacts. When the conditional DiT is computed at the current step but the unconditional noise prediction is reused from a previous step, the two predictions come from

Table 1: Spearman’s correlation (ρ) between proxy candidates and oracle. Optimal proxies are bolded.

Proxy	Cosmos-Predict2-2B	Wan2.1-1.3B	Wan2.1-14B
① block in	0.16	0.35	0.00
② attn in	0.45	0.35	0.02
③ attn out	-0.07	0.60	0.65
④ cross attn in	0.32	0.35	0.03
⑤ cross attn out	0.68	0.89	0.53
⑥ mlp in	0.64	0.40	0.16
⑦ mlp out	0.82	0.40	0.21
⑧ block out	0.51	0.40	0.13

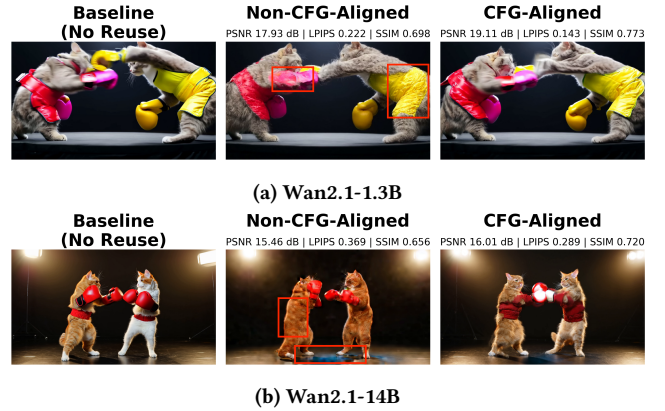


Figure 5: Impact of CFG alignment on visual quality. Visual artifacts in the non-CFG-aligned video is highlighted. Best viewed zoomed in.

slightly different noise levels. Since CFG combines these predictions (Algorithm 1, line 16), this mismatch fails to steer the diffusion process from low-quality outputs, producing visual artifacts.

Figure 5 illustrates this phenomenon at a high reuse ratio to amplify visual differences, though the effect persists at lower ratios (quantified in Section 4.3). In the non-aligned approach, the clothing in Figure 5a appears less vibrant, while the fur and floor in Figure 5b show blurriness and anomalous artifacts. In contrast, both the baseline and CFG-aligned versions preserve fine details such as fur texture.

To address this, we propose guidance-aligned reuse: the proxy from the first DiT block of the conditional pass (line 3 of Algorithm 1) determines whether to reuse at each step. Crucially, both conditional and unconditional passes then either compute or reuse together (lines 7&8 and 11&13). This synchronization ensures the guided noise prediction in line 16 receives matching inputs from both passes, eliminating visual artifacts caused by misalignment.

4 Evaluation

4.1 Experimental Setup

We evaluate GALAXYDiT on three state-of-the-art DiT-based video diffusion models representing different scales, architectures, and modalities. Wan2.1-1.3B and Wan2.1-14B [16] are leading text-to-video (T2V) models widely used in artistic content generation.

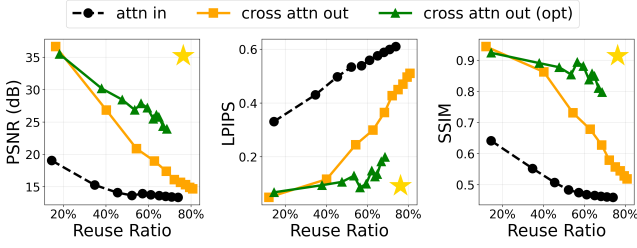


Figure 6: Ablation of proxy selection for Wan2.1-1.3B. Cross attn out (opt) uses cross attn out as the proxy and excludes the first 20% of denoising steps from reuse. The star marks the optimal corner with higher quality and reuse.

Cosmos-Predict2-2B [10] is a foundation model targeting physical world simulation. It is an image-to-video (I2V) model, which generates a video from an initial frame and a text prompt. Wan2.1 models use 50 denoising steps while Cosmos-Predict2 uses 36 steps. For each model, we select the optimal proxy using statistics collected on 16 prompts as described in Section 3.2, then determine representative thresholds for different quality-latency trade-offs.

We evaluate Wan2.1 models on all 1330 prompts from the VBench-2.0 suite [23], and Cosmos-Predict2 on the 1118 image-prompt pairs from the VBench(beta)-I2V dataset [3, 4]. Latency is measured on 1 A100 GPU for Wan2.1-1.3B and Cosmos-Predict2, and 8 A100s for Wan2.1-14B.

The baseline is the original model [11, 16] with full computation. Baseline-generated videos serve as references for computing PSNR, SSIM, and LPIPS. VBench-2.0 scores are computed using the official implementation.

4.2 Ablation on Reuse Metric Selection

We ablate proxy selection on Wan2.1-1.3B using a random subset of VBench-2.0 prompts with CFG-aligned mode. We compare three configurations: attn in, cross attn out, and cross attn out (opt). The purpose of this ablation is to conclude if our Spearman’s coefficient-based selection criterion leads to higher video quality.

Based on Spearman’s coefficients in Table 1, attn in correlates weakly with the oracle ($\rho = 0.35$), while cross attn out shows strong order-preservation ($\rho = 0.89$). Figure 6 confirms that the video quality using the optimal proxy is higher: cross attn out achieves up to 15 dB higher PSNR at lower reuse ratios, with further improvement at high reuse when excluding initial steps.

4.3 Ablation on CFG-Alignment

Using the optimal reuse metric identified in Section 4.2, cross attn out (opt), we compare CFG-aligned versus non-aligned approaches on the same VBench-2.0 subset for Wan2.1-1.3B.

The conventional approach determines reuse independently for conditional and unconditional passes at each step. Our CFG-aligned approach synchronizes these decisions: reuse always occurs simultaneously for both passes.

As shown in Figure 7, CFG alignment achieves 4 dB higher PSNR, 10% lower perceptual loss, and 10% higher structural similarity at 60% reuse, confirming the visual motivation in Figure 5.

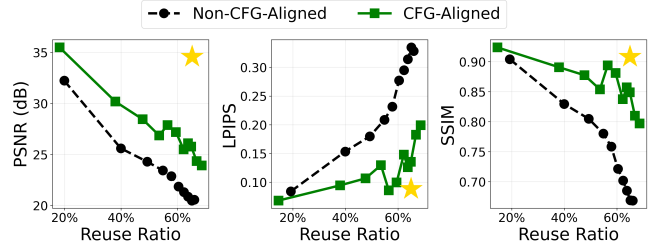


Figure 7: Ablation of guidance alignment in Wan2.1-1.3B. Alignment improves all quality metrics across reuse rates.

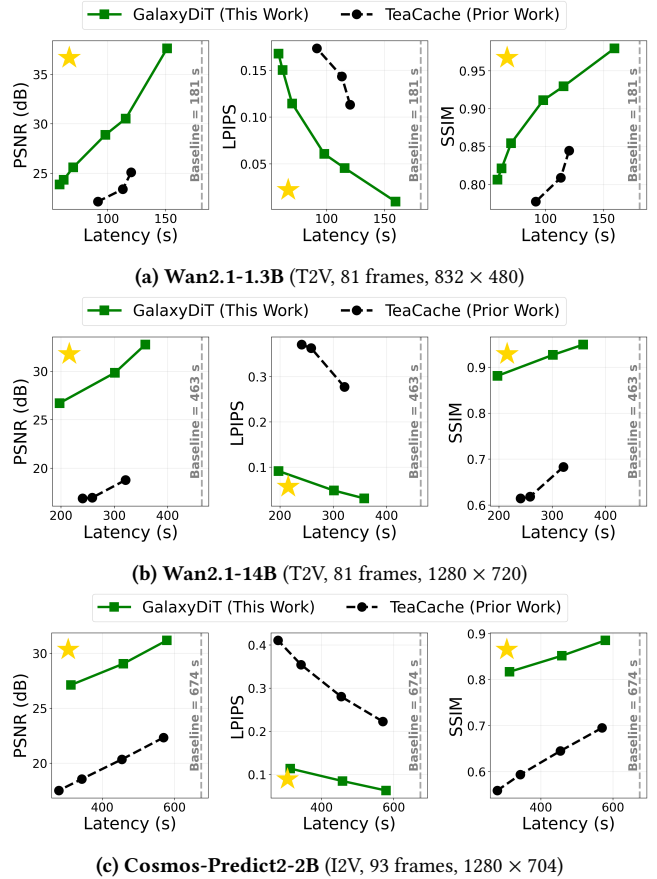


Figure 8: Quality-latency comparison of GALAXYDiT against prior work [7] and the full-compute baseline. GALAXYDiT achieves superior quality at equivalent speedup across T2V and I2V modalities. The yellow star indicates the optimal corner.

4.4 Quality and Speedup

Selecting different thresholds trades off video quality for speed. GALAXYDiT-fast uses higher thresholds for maximum speedup, while GALAXYDiT-slow prioritizes quality, which is suitable for quality-sensitive applications like robotics simulation.

Method	Speedup \uparrow	PSNR \uparrow	LPIPS \downarrow	SSIM \uparrow	VBench-2.0 \uparrow
Wan2.1-1.3B (81 frames, 832 \times 480)					
Baseline	1.00 \times	—	—	—	56.65%
TeaCache-slow	1.51 \times	25.1 dB	0.113	0.845	55.39% (−1.26%)
TeaCache-fast	1.98 \times	22.1 dB	0.173	0.777	52.91% (−3.74%)
GalaxyDiT-slow	1.85 \times	28.9 dB	0.061	0.911	55.68% (−0.97%)
GalaxyDiT-fast	2.57\times	25.6 dB	0.114	0.854	52.83% (−3.82%)
Wan2.1-14B (81 frames, 1280 \times 720)					
Baseline	1.00 \times	—	—	—	58.36%
TeaCache-slow	1.45 \times	18.8 dB	0.277	0.683	58.79% (+0.43%)
TeaCache-fast	1.93 \times	16.9 dB	0.371	0.615	57.61% (−0.75%)
GalaxyDiT-slow	1.30 \times	32.7 dB	0.031	0.949	59.22% (+0.86%)
GalaxyDiT-medium	1.54 \times	29.8 dB	0.048	0.927	58.05% (−0.31%)
GalaxyDiT-fast	2.37\times	26.6 dB	0.093	0.881	57.64% (−0.72%)

Table 2: Performance comparison of GalaxyDiT against prior works on Wan2.1 models.

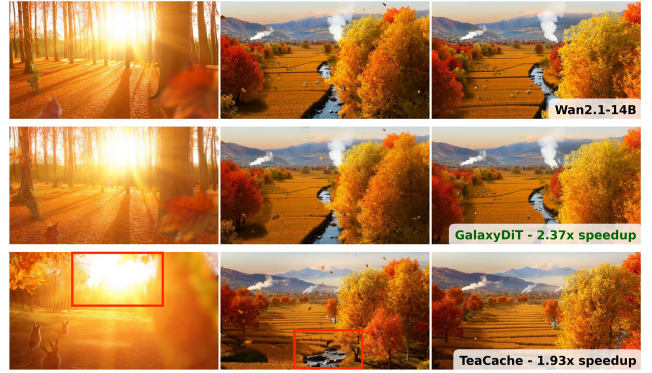
At matched quality (25.6 dB PSNR, 0.11 LPIPS, and 0.85 SSIM), GALAXYDiT achieves 1.74 \times speedup over prior work and 2.57 \times over baseline on Wan2.1-1.3B (Figure 8a). At matched latency, GALAXYDiT delivers 6 dB higher PSNR, 10% lower perceptual loss, and 10% higher structural similarity. This trend holds across scales: on Wan2.1-14B, GALAXYDiT maintains above 26.6 dB PSNR, 88% SSIM, and below 9.3% LPIPS at 2.37 \times speedup. This trend also holds across model families: on Cosmos-Predict2, at the same speedup, GALAXYDiT achieves 9 dB higher PSNR, 10% lower LPIPS and 20% higher SSIM.

We evaluate on VBench-2.0 rather than VBench-1.0 because recent models have saturated VBench-1.0’s superficial metrics, and emerging applications require the intrinsic faithfulness attributes, including physical law adherence, commonsense reasoning, and compositional integrity, which are measured by VBench-2.0 [23]. As tested on the VBench-2.0 prompts, even GALAXYDiT-fast exceeds the fidelity of prior work’s slow variant while delivering 2.57 \times (1.3B) and 2.37 \times (14B) speedups (Table 2). Notably, GALAXYDiT-slow improves the base 14B model’s VBench-2.0 score by +0.8%.

4.5 Visual Comparison

Figure 1 and Figure 9 show example videos from VBench-2.0 prompts. In both scenarios, GALAXYDiT closely resembles the baseline. The missing planetary details in TeaCache’s version (Figure 1) contribute to its low PSNR, since PSNR measures pixel-level fidelity. Similarly in Figure 9, tree details basked in the sunlight are preserved in GALAXYDiT but lost in prior work. SSIM captures structural similarity, and both examples show that the structural composition of the prior work is different from the base model, despite using the same noised latent.

Beyond fidelity, TeaCache exhibits worse prompt adherence. The space station prompt specifies astronauts with faces “reflecting curiosity and amazement,” yet TeaCache omits one astronaut entirely while the other faces away from camera. This degradation likely stems from the non-CFG-aligned method, given that CFG is essential for prompt adherence.



Prompt: The camera enters a golden autumn forest, where the leaves have turned brilliant shades from gold to orange-red. A few leaves drift down with the wind. **Sunlight filters through the gaps in the trees**, casting dappled spots of light on the forest floor. **The scene shifts** to a field outside the forest, where ripe rice stalks sway in the breeze, their golden heads bowing under the weight of the grain... The camera moves again to **a winding stream**...

Figure 9: Qualitative comparison on a complex landscape scene with Wan2.1-14B. Best viewed zoomed in.

4.6 Memory Efficiency

We analyze memory overhead of the 14B model as it represents the most memory-constrained scenario. The model itself contains 28 GB of parameters, with the text encoder requiring an additional 20 GB that can be offloaded during diffusion [16].

GALAXYDiT stores four tensors: residuals from the previous step ($\text{res}_{S-1, \text{cond}}$ and $\text{res}_{S-1, \text{uncond}}$), the current pass input for residual calculation ($y_{\text{in}, S, \text{current pass}}$), and the conditional proxy for computing the next reuse metric ($\text{proxy}_{S, \text{cond}}$). For a sequence length of 75600, this amounts to 2.88 GB of GPU memory.

For single-GPU inference (e.g., A100 40 GB or 80 GB), memory is critical. RADiT [12] stores tensors at every layer (173 GB), making it prohibitively expensive, while TeaCache [7] requires 3.6 GB for embedded inputs and cached tensors. GALAXYDiT achieves the lowest memory overhead among reuse-based acceleration methods.

5 Conclusion

We presented GALAXYDiT, a training-free method to accelerate video diffusion transformers through guidance alignment and adaptive proxy-based reuse. By systematically selecting optimal proxies for each model using rank-order correlation analysis, we ensure that reuse decisions align with the true importance of each denoising step. Our guidance-aligned reuse strategy eliminates visual artifacts inherent in CFG-agnostic approaches. Evaluated on Wan2.1-1.3B and Wan2.1-14B, GalaxyDiT achieves 1.87 \times and 2.37 \times speedup with only 0.97% and 0.72% drop on the VBench-2.0 benchmark, respectively. With both the T2V Wan2.1 models and the I2V Cosmos-Predict2, GALAXYDiT achieves high fidelity to the base model, 5 to 10 dB higher PSNR than prior works at equivalent speedups. With model-specific proxy selection and CFG-aware reuse, GALAXYDiT enables downstream applications with efficient and high-quality video generation.

Acknowledgments

The authors would like to thank Weili Nie, Reena Elangovan, Marina Neseem, Charbel Sakr, Celine Lin, Rangharajan Venkatesan, Xiao Fu, Akshat Ramachandran, Jianming Tong, Jacob Ridgway and Bryan Foo for insightful discussions.

References

- [1] Jonathan Ho and Tim Salimans. 2022. Classifier-Free Diffusion Guidance. doi:10.48550/arXiv.2207.12598 arXiv:2207.12598 [cs].
- [2] Jonathan Ho, Tim Salimans, Alexey Gritsenko, William Chan, Mohammad Norouzi, and David J. Fleet. 2022. Video Diffusion Models. doi:10.48550/arXiv.2204.03458 arXiv:2204.03458 [cs].
- [3] Ziqi Huang, Fan Zhang, Xiaojie Xu, Yinan He, Jiashuo Yu, Ziyue Dong, Qianli Ma, Nattapol Chanpaisit, Chenyang Si, Yuming Jiang, Yaohui Wang, Xinyuan Chen, Ying-Cong Chen, Limin Wang, Dahua Lin, Yu Qiao, and Ziwei Liu. 2024. VBench++: Comprehensive and Versatile Benchmark Suite for Video Generative Models. doi:10.48550/arXiv.2411.13503 arXiv:2411.13503 [cs].
- [4] Ziqi Huang, Fan Zhang, Xiaojie Xu, Yinan He, Jiashuo Yu, Ziyue Dong, Qianli Ma, Nattapol Chanpaisit, Chenyang Si, Yuming Jiang, Yaohui Wang, Xinyuan Chen, Ying-Cong Chen, Limin Wang, Dahua Lin, Yu Qiao, and Ziwei Liu. 2024. VBench-I2V (Beta Version). https://github.com/Vchitect/VBench/tree/master/vbench2_beta_i2v arXiv:2411.13503 [cs].
- [5] Hunyuan Foundation Model Team. 2025. HunyuanVideo: A Systematic Framework For Large Video Generative Models. doi:10.48550/arXiv.2412.03603
- [6] Yaron Lipman, Ricky T. Q. Chen, Heli Ben-Hamu, Maximilian Nickel, and Matt Le. 2023. Flow Matching for Generative Modeling. doi:10.48550/arXiv.2210.02747 arXiv:2210.02747 [cs].
- [7] Feng Liu, Shiwei Zhang, Xiaofeng Wang, Yujie Wei, Haonan Qiu, Yuzhong Zhao, Yingya Zhang, Qixiang Ye, and Fang Wan. 2025. Timestep Embedding Tells: It's Time to Cache for Video Diffusion Model. doi:10.48550/arXiv.2411.19108 arXiv:2411.19108 [cs].
- [8] Xingchao Liu, Chengyue Gong, and Qiang Liu. 2022. Flow Straight and Fast: Learning to Generate and Transfer Data with Rectified Flow. doi:10.48550/arXiv.2209.03003 arXiv:2209.03003 [cs].
- [9] Zhengyao Lv, Chenyang Si, Junhao Song, Zhenyu Yang, Yu Qiao, Ziwei Liu, and Kwan-Yee K. Wong. 2025. FasterCache: Training-Free Video Diffusion Model Acceleration with High Quality. doi:10.48550/arXiv.2410.19355 arXiv:2410.19355 [cs].
- [10] NVIDIA. 2025. Cosmos-Predict2. <https://github.com/nvidia-cosmos/cosmos-predict2>
- [11] NVIDIA. 2025. Cosmos World Foundation Model Platform for Physical AI. doi:10.48550/arXiv.2501.03575
- [12] Youngjun Park and Sangyeon Kim. 2025. RADiT: Redundancy-Aware Diffusion Transformer Acceleration Leveraging Timestep Similarity. In *DAC*.
- [13] William Peebles and Saining Xie. 2023. Scalable Diffusion Models with Transformers. doi:10.48550/arXiv.2212.09748 arXiv:2212.09748 [cs].
- [14] Xiangyu Peng, Zangwei Zheng, Chenhui Shen, Tom Young, Xinying Guo, Binluo Wang, Hang Xu, Hongxin Liu, Mingyan Jiang, Wenjun Li, Yuhui Wang, Anbang Ye, Gang Ren, Qianran Ma, Wanying Liang, Xiang Lian, Xiwen Wu, Yuting Zhong, Zhuangyan Li, Chaoyu Gong, Guojun Lei, Leijun Cheng, Limin Zhang, Minghao Li, Ruijie Zhang, Silan Hu, Shijie Huang, Xiaokang Wang, Yuanheng Zhao, Yuqi Wang, Ziang Wei, and Yang You. 2025. Open-Sora 2.0: Training a Commercial-Level Video Generation Model in \$200k. doi:10.48550/arXiv.2503.09642 arXiv:2503.09642 [cs].
- [15] Robin Rombach, Andreas Blattmann, Dominik Lorenz, Patrick Esser, and Björn Ommer. 2022. High-Resolution Image Synthesis with Latent Diffusion Models. doi:10.48550/arXiv.2112.10752 arXiv:2112.10752 [cs].
- [16] Team Wan. 2025. Wan: Open and Advanced Large-Scale Video Generative Models. doi:10.48550/arXiv.2503.20314
- [17] Haocheng Xi, Shuo Yang, Yilong Zhao, Chenfeng Xu, Muiyang Li, Xiuyu Li, Yujun Lin, Han Cai, Jintao Zhang, Dacheng Li, Jianfei Chen, Ion Stoica, Kurt Keutzer, and Song Han. 2025. Sparse VideoGen: Accelerating Video Diffusion Transformers with Spatial-Temporal Sparsity. doi:10.48550/arXiv.2502.01776 arXiv:2502.01776 [cs].
- [18] Zhuoyi Yang, Jiayan Teng, Wendi Zheng, Ming Ding, Shiyu Huang, Jiazheng Xu, Yuanming Yang, Wenyi Hong, Xiaohan Zhang, Guanyu Feng, Da Yin, Yuxuan Zhang, Weihao Wang, Yean Cheng, Bin Xu, Xiaotao Gu, Yuxiao Dong, and Jie Tang. 2025. CogVideoX: Text-to-Video Diffusion Models with An Expert Transformer. doi:10.48550/arXiv.2408.06072 arXiv:2408.06072 [cs].
- [19] Zhihang Yuan, Hanling Zhang, Pu Lu, Xuefei Ning, Linfeng Zhang, Tianchen Zhao, Shengren Yan, Guohao Dai, and Yu Wang. 2024. DiTFastAttn: Attention Compression for Diffusion Transformer Models. doi:10.48550/arXiv.2406.08552 arXiv:2406.08552 [cs].
- [20] Yuanhao Zhai, Kevin Lin, Zhengyuan Yang, Linjie Li, Jianfeng Wang, Chung-Ching Lin, David Doermann, Junsong Yuan, and Lijuan Wang. 2024. Motion Consistency Model: Accelerating Video Diffusion with Disentangled Motion-Appearance Distillation. In *38th Conference on Neural Information Processing Systems*.
- [21] Haiyu Zhang, Xinyuan Chen, Yaohui Wang, Xihui Liu, Yunhong Wang, and Yu Qiao. 2025. AccVideo: Accelerating Video Diffusion Model with Synthetic Dataset. doi:10.48550/arXiv.2503.19462 arXiv:2503.19462 [cs].
- [22] Richard Zhang, Phillip Isola, Alexei A. Efros, Eli Shechtman, and Oliver Wang. 2018. The Unreasonable Effectiveness of Deep Features as a Perceptual Metric. doi:10.48550/arXiv.1801.03924 arXiv:1801.03924 [cs].
- [23] Dian Zheng, Ziqi Huang, Hongbo Liu, Kai Zou, Yinan He, Fan Zhang, Lulu Gu, Yuanhan Zhang, Jingwen He, Wei-Shi Zheng, Yu Qiao, and Ziwei Liu. 2025. VBench-2.0: Advancing Video Generation Benchmark Suite for Intrinsic Faithfulness. doi:10.48550/arXiv.2503.21755 arXiv:2503.21755 [cs].